

# Mask Image Watermarking

**Runyi Hu<sup>1</sup>, Jie Zhang<sup>2\*</sup>, Shiqian Zhao<sup>1</sup>, Nils Lukas<sup>3</sup>,  
Jiwei Li<sup>4</sup>, Qing Guo<sup>2</sup>, Han Qiu<sup>5</sup>, Tianwei Zhang<sup>1</sup>**

<sup>1</sup>Nanyang Technological University    <sup>2</sup>CFAR and IHPC, A\*STAR, Singapore  
<sup>3</sup>MBZUAI    <sup>4</sup>Zhejiang University    <sup>5</sup>Tsinghua University

{runyi.hu, tianwei.zhang}@ntu.edu.sg

{zhang\_jie}@cfar.a-star.edu.sg

<https://github.com/hurunyi/MaskMark>

## Abstract

We present MaskMark, a simple, efficient and flexible framework for image watermarking. MaskMark has two variants: MaskMark-D, which supports global watermark embedding, watermark localization, and local watermark extraction for applications such as tamper detection, and MaskMark-ED, which focuses on local watermark embedding and extraction with enhanced robustness in small regions, enabling localized image protection. Built upon the classical Encoder-Distortion-Decoder training paradigm, MaskMark-D introduces a simple masking mechanism during the decoding stage to support both global and local watermark extraction. A mask is applied to the watermarked image before extraction, allowing the decoder to focus on selected regions and learn local extraction. A localization module is also integrated into the decoder to identify watermark regions during inference, reducing interference from irrelevant content and improving accuracy. MaskMark-ED extends this design by incorporating the mask into the encoding stage as well, guiding the encoder to embed the watermark in designated local regions for enhanced robustness. Comprehensive experiments show that MaskMark achieves state-of-the-art performance in global watermark extraction, local watermark extraction, watermark localization, and multi-watermark embedding. It outperforms all existing baselines, including the recent leading model WAM for local watermarking, while preserving high visual quality of the watermarked images. MaskMark is also flexible, by adjusting the distortion layer, it can adapt to different robustness requirements with just a few steps of fine-tuning. Moreover, our approach is efficient and easy to optimize, requiring only 20 hours on a single A6000 GPU with just 1/15 the computational cost of WAM.

## 1 Introduction

Image watermarking (Potdar et al., 2005) is a crucial technique for embedding imperceptible information into images, serving purposes such as copyright protection, content authentication, and provenance tracking. With the proliferation of AI-generated content (AIGC) (Rombach et al., 2022; Saharia et al., 2022), the necessity of robust watermarking schemes has become even more pronounced, as distinguishing between real and synthetic images is increasingly challenging.

Traditional deep image watermarking methods (Zhu et al., 2018; Tancik et al., 2020; Jia et al., 2021) typically perform global watermark embedding and extraction, treating the entire image as a uniform entity. However, this global approach suffers from several critical limitations. First, when the image undergoes heavy tampering, such as inpainting (Yu et al., 2023; Zhang et al., 2023), resulting

\*The corresponding author

in only a small region retaining the watermark, global methods often fail to extract it effectively. Second, even if a watermark is successfully extracted from the entire image, such methods cannot localize which region actually contains the watermark, making fine-grained forensic analysis and fair judgment difficult. Third, in scenarios where only specific regions of an image are valuable and need protection, or when different parts of the image originate from different sources and require distinct watermarking, global embedding is inherently incapable of providing the flexibility and granularity.

To address these limitations, we propose MaskMark, a simple, efficient, and flexible image watermarking framework that introduces a masking mechanism during training to guide the embedding and extraction of localized watermark signals. Depending on which stage the mask is introduced, MaskMark has two variants. **MaskMark-D** introduces the mask only during the decoding phase. This design enables global watermark embedding while supporting localized extraction. Specifically, by applying masks over the watermarked images before watermark extraction, the decoder learns to extract watermark signals from specific regions. Meanwhile, the end-to-end training encourages the encoder to embed the watermark uniformly across the image, ensuring that all regions contain sufficient signal for reliable local extraction. Additionally, a watermark localization module is incorporated into the decoder, enabling it to identify watermarked regions during inference, which also reduces interference from irrelevant content and enhances practical robustness. **MaskMark-ED** introduces the mask during both the encoding and decoding phases, allowing for both localized watermark embedding and extraction. In this setting, the encoder is trained to embed not only the watermark bits but also the spatial mask into the image. This enables the model to adaptively allocate watermark strength to designated regions while leaving the rest of the image nearly untouched.

Extensive experiments demonstrate that MaskMark significantly outperforms existing baselines in both global and local watermark extraction, as well as in watermark localization, while preserving image quality. Under the 32-bit embedding setting, MaskMark achieves near-perfect accuracy in global watermark extraction, even under common distortions. Notably, geometric distortions cause most baseline methods to fail completely, while MaskMark remains highly robust. For local watermark extraction, MaskMark consistently delivers strong results: when only 5% of the image carries watermark signals and no distortion is applied, it achieves nearly 100% extraction accuracy, and remains robust across a wide range of distortion scenarios. In terms of watermark localization, MaskMark demonstrates high precision, accurately identifying watermark regions even in the presence of various distortions. Furthermore, although not explicitly trained for multi-watermark embedding, MaskMark maintains high extraction and localization performance even when the number of embedded watermarks increases to five. In addition to its effectiveness, MaskMark is highly efficient. Training requires only a single A6000 GPU for approximately 20 hours, 15 $\times$  less compute than the recent state-of-the-art local watermarking model WAM (Sander et al., 2025). It also scales effortlessly to higher bit lengths (e.g., 64 or 128), retaining strong local extraction performance even under distortion, whereas WAM is inherently limited to 32-bit embedding and does not scale beyond that. Furthermore, the framework supports fast fine-tuning for different applications: for example, after just 20k training steps, MaskMark can reach over 99% extraction accuracy against VAE-based adaptive attacks. These advantages make MaskMark a practical, efficient, and scalable solution for real-world watermarking applications. In summary, our main contributions are as follows:

- We introduce MaskMark, a simple yet powerful image watermarking framework that supports both global and local embedding and extraction, along with watermark localization via a flexible masking mechanism.
- Extensive experiments demonstrate MaskMark excels in global and local extraction, as well as multi-watermark embedding, while maintaining high visual quality of the watermarked images.
- MaskMark is highly efficient, requiring 15 $\times$  less compute than WAM, seamlessly scales to higher watermark bit lengths (e.g., 64 or 128), and supports fast fine-tuning for quick adaptation to different attack scenarios, enhancing its practicality.

## 2 Background

### 2.1 Image Watermarking

Image watermarking techniques can generally be categorized into two types: *global watermarking* and *local watermarking* methods. **Global watermarking methods aim to extract watermark**

**information from the entire image.** Most traditional deep learning-based approaches fall into this category. These methods focus on achieving robustness against various types of distortions, ensuring that the embedded watermark can still be reliably recovered even when the image undergoes degradation. For example, MBRS (Jia et al., 2021) specifically targets robustness against JPEG compression. Methods like StegaStamp (Tancik et al., 2020) and PIMoG (Fang & et al., 2022) are designed to handle real-world physical distortions such as screen-shooting and print-shooting. More recent approaches like ZoDiac (Zhang et al., 2024a) and SuperMark (Hu et al., 2024a) tackle adaptive attacks, while Robust-Wide (Hu et al., 2024b) and VINE (Lu et al., 2024) focus on robustness against instruction-driven image editing.

**In contrast, local watermarking methods focus on extracting watermark information from a specific region of the image.** Recent methods, such as WAM (Sander et al., 2025) and our proposed MaskMark, belong to this category. WAM treats watermark extraction as a segmentation task (Kirillov et al., 2023), predicting watermark bits at the pixel level. This fine-grained approach enables precise local extraction but also introduces challenges. As the predicted bit length per pixel increases (e.g., beyond 32 bits), the task becomes more difficult, causing training instability and reduced performance. Additionally, WAM’s training is computationally expensive, requiring eight V100 GPUs for nearly a week, making it impractical for widespread use. Moreover, WAM does not support native local watermark embedding; instead, it globally embeds a watermark and then crops the image to focus on the local region, introducing inherent losses during embedding that weaken the robustness of final extraction.

## 2.2 Watermark Localization

Watermark localization (Zhang et al., 2024b; Hu et al., 2025; Sander et al., 2025) refers to the ability to determine which regions of a watermarked image still contain watermark information after modifications. This capability enables the identification of unaltered content, serving as an active detection mechanism for tamper localization. Currently, image watermarking techniques primarily adopt two paradigms for watermark localization. **The first paradigm embeds a one-dimensional copyright watermark alongside a two-dimensional localization watermark in the original image.** During extraction, localization is based on the fragility of the localization watermark, which cannot be fully recovered from a modified image. Key methods in this category include EditGuard (Zhang et al., 2024b) and OmniGuard (Zhang et al., 2024c). EditGuard embeds a solid-color template within the host image and attempts to recover it from a modified version. The difference between the recovered and original templates is calculated at each pixel, and a threshold-based decision identifies watermark-preserved regions. OmniGuard improves upon EditGuard by embedding a natural image as the template, enhancing fidelity. It also introduces a Degradation-aware Tamper Extractor, improving robustness in detecting tampered regions under distortion. This paradigm requires parallel extraction of both copyright and localization watermarks, which may affect image quality. Moreover, both watermarks need independent robustness, and the presence of the template watermark does not guarantee the presence of the copyright watermark.

**The second paradigm, in contrast, embeds only a one-dimensional copyright bitstream and directly determines the presence or absence of watermark information at each pixel to achieve localization.** Methods such as WAM (Sander et al., 2025) and our proposed MaskMark fall under this category. WAM employs a decoder that simultaneously performs pixel-wise watermark presence detection and copyright bit extraction. In contrast, our MaskMark incorporates a dedicated localization module within the decoder, focusing solely on watermark presence detection at each pixel. This approach is more lightweight and easier to optimize. Compared to the first paradigm, this method ensures that the localized watermark regions strictly correspond to the areas containing copyright watermark information, enhancing interpretability. Additionally, it guarantees both the robustness of copyright watermark extraction and the robustness of localization.

## 3 Methodology

### 3.1 Design Principles

In general, our objective is to enable the watermark model to effectively extract watermarks from images where only local regions are watermarked. We identify three primary reasons why traditional watermark models fail in this scenario. First, the decoder is trained exclusively on globally water-

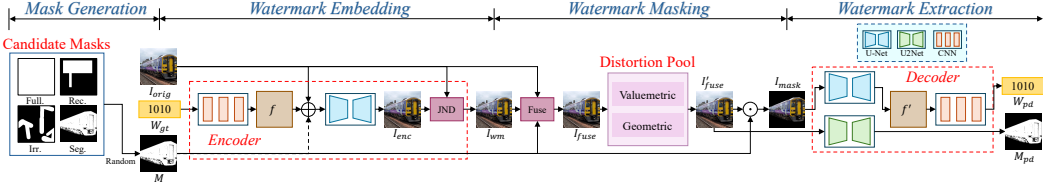


Figure 1: The overall end-to-end training pipeline of MaskMark. (1) In the **Mask Generation** stage, we generate candidate masks from four predefined types and randomly select one mask  $M$  for the subsequent stages. (2) In the **Watermark Embedding** stage, the encoder  $\mathcal{E}$  embeds the watermark bits  $W_{gt}$  into the original image  $I_{orig}$ , optionally using the mask  $M$  (for MaskMark-ED), to produce the watermarked image  $I_{wm}$ . (3) In the **Watermark Masking** stage, the mask  $M$  is used to fuse  $I_{orig}$  and  $I_{wm}$ , resulting in the fused image  $I_{fuse}$ , which is then subjected to a randomly selected distortion from a predefined distortion pool, yielding the distorted image  $I'_fuse$ . The masked region is then cropped using  $M$  to obtain  $I_{mask}$ . (4) In the **Watermark Extraction** stage, the decoder  $\mathcal{D}$  extracts the predicted watermark bits  $W_{pd}$  from  $I_{mask}$  and the predicted mask  $M_{pd}$  from  $I'_fuse$ .

marked images and has never encountered cases where only a local region contains a watermark. Consequently, it is unable to perform zero-shot extraction when presented with such images. Second, the non-watermarked portions of an image interfere with the decoder’s extraction process, especially when the watermark occupies a small area, leading to extraction failure. Third, because the decoder is optimized for global watermark extraction, the encoder tends to dilute the watermark’s intensity over the entire image. This results in local regions having either insufficient or fragmented watermark strength, thereby exacerbating the extraction challenge.

To address these challenges, we find that simply incorporating a basic mask mechanism during the *decoding stage* to manipulate the watermarked image generated by the encoder is sufficient. To solve the first issue, we retain only the watermark in the regions selected by the mask while setting the pixel values of the remaining regions to zero, thereby training the decoder to extract watermarks from partially watermarked images. To overcome the second issue, we replace the non-masked regions with the original clean image and incorporate a watermark localization module in the decoder. This module learns to differentiate between watermarked and non-watermarked regions, effectively mitigating the interference from irrelevant image content. These two strategies directly address the first and second challenges and indirectly resolve the third challenge. By ensuring that the decoder can extract the watermark from local regions and accurately distinguish it from non-watermarked areas, the encoder is encouraged to distribute the watermark strength uniformly across all local regions rather than diluting it over the entire image, thereby preserving both extractability and distinctiveness.

The strategies above form the basis of our MaskMark-D. To further enhance the encoder’s ability to address the third challenge directly, we propose MaskMark-ED, which also introduces the mask mechanism during the *encoding stage*. In MaskMark-ED, the mask is embedded into the image along with the watermark bits during training. This enables the encoder to learn to actively concentrate the watermark within the selected regions based on the embedded mask, thereby further improving the robustness of local watermarking.

### 3.2 Overview

The overall end-to-end training pipeline is shown in Figure 1. It consists of four stages: (1) Mask Generation, (2) Watermark Embedding, (3) Watermark Masking, and (4) Watermark Extraction. In the following, we provide a detailed description of each stage.

### 3.3 Mask Generation

The mask generation process constructs a pool of candidate masks with diverse types, from which one is randomly selected as the mask  $M$  for each image during training. We follow a similar mask generation strategy as LaMa (Suvorov et al., 2022), utilizing four distinct types of masks: Full Mask, Rectangle Mask, Irregular Mask, and Segment Mask. These masks are designed to enhance the model’s ability to handle watermark embedding and extraction under diverse conditions, and

each serves a specific purpose: The **Full Mask** enables global watermark learning across the entire image, serving as a fundamental capability. The **Rectangle Mask** focuses on regularly shaped local regions, encouraging the model to operate within confined areas of varying sizes. The **Irregular Mask** introduces complex, arbitrarily shaped regions to improve robustness in non-uniform contexts. Lastly, the **Segment Mask** targets semantically meaningful areas by leveraging object masks from the MS-COCO dataset (Lin et al., 2014), helping the model generalize to real-world scenarios.

### 3.4 Watermark Embedding

We describe our method for embedding both the watermark bits  $W_{gt}$  and the optional mask  $M$  into the original image  $I_{orig}$ . The process begins by randomly sampling binary watermark bits  $W_{gt} \in \{0, 1\}$  of length  $l$ . These bits are then transformed into a feature map  $f$  with shape  $(C_f, H, W)$  using a lightweight CNN, where  $C_f$  represents the number of channels in the feature map. This CNN consists of a linear layer followed by several Conv-Norm-ReLU blocks. Specifically, the linear layer first maps  $W_{gt}$  to a tensor of shape  $(1, l, l)$ , which is then bilinearly interpolated to match the spatial dimensions of the input image, resulting in a tensor of shape  $(1, H, W)$ . This tensor is then processed through the CNN to produce the feature map  $f$ .

To embed the watermark, we begin by concatenating the original image  $I_{orig}$  with the watermark feature  $f$  along the channel dimension. For the MaskMark-D variant, no further concatenation is performed, resulting in a tensor of shape  $(3 + C_f, H, W)$  that encourages global watermark embedding. In contrast, the MaskMark-ED variant additionally concatenates the mask  $M$ , yielding a tensor of shape  $(3 + C_f + 1, H, W)$ . The inclusion of  $M$  serves to guide the model toward localized embedding by indicating regions of interest during training. The use cases for both variants are discussed in detail in Sec. 3.8.

The concatenated tensor is then passed through a U-Net (Kirillov et al., 2023) to generate an intermediate encoded image  $I_{enc}$ . To obtain the final watermarked image  $I_{wm}$ , we apply a Just-Noticeable-Difference (JND) module (Wu et al., 2017), which modulates the embedding signal based on human visual sensitivity to enhance perceptual quality:

$$I_{wm} = I_{orig} + \mu \times \text{JND}(I_{enc} - I_{orig}), \quad (1)$$

where  $\mu$  is the JND scaling factor to control the watermark strength. We explore several strategies to improve the visual quality of the watermarked image and find that JND modulation consistently delivers the best performance (see Sec. 4.5 for details).

### 3.5 Watermark Masking

We describe how the mask  $M$  is used to process the watermarked image  $I_{wm}$  for subsequent mask prediction and watermark extraction by the decoder.

First, we generate a fused image  $I_{fuse}$  by combining  $I_{wm}$  and the original image  $I_{orig}$ , where the unmasked regions are replaced with the corresponding pixels from  $I_{orig}$ :

$$I_{fuse} = I_{wm} \odot M + I_{orig} \odot (1 - M). \quad (2)$$

Next, we apply a randomly selected distortion from a predefined distortion pool to  $I_{fuse}$ , producing an augmented image  $I'_{fuse}$ . This step follows a common practice in traditional watermarking methods to improve robustness against various transformations.

Finally, we use the mask  $M$  once more to isolate the watermarked regions of  $I'_{fuse}$ , setting all other pixels to zero to obtain the input  $I_{mask}$  for watermark extraction:

$$I_{mask} = I'_{fuse} \odot M. \quad (3)$$

### 3.6 Watermark Extraction

We describe how the decoder  $\mathcal{D}$  extracts the predicted mask from  $I'_{fuse}$  and recovers the watermark bits from  $I_{mask}$ . To achieve these two objectives,  $\mathcal{D}$  consists of two dedicated modules: a U<sup>2</sup>-Net (Qin et al., 2020) for mask prediction, and a U-Net (Ronneberger et al., 2015) followed by a CNN for watermark extraction.

Specifically, the U<sup>2</sup>-Net takes  $I'_{fuse}$  as input and predicts a mask  $M_{pd}$  of shape  $(C_M, H, W)$ . Meanwhile, the U-Net processes  $I_{mask}$  to produce an intermediate feature  $f'$  with shape  $(C_f, H, W)$ , which is then passed through a CNN to obtain the predicted watermark bits  $W_{pd}$ . Unlike the CNN used in the encoder  $\mathcal{E}$ , the CNN in the decoder  $\mathcal{D}$  first applies several Conv–Norm–ReLU layers to further extract features from  $f'$ . The resulting features are then interpolated to a fixed shape of  $(1, l, l)$  and subsequently transformed by linear layers into a bit sequence of length  $l$ , yielding the final watermark prediction  $W_{pd}$ .

### 3.7 Training Objectives

For all loss functions, we use Mean Squared Error (MSE). Specifically, the encoder loss is defined as:

$$\mathcal{L}_{enc} = \mathcal{L}_{MSE}(I_{wm}, I_{orig}). \quad (4)$$

Note that we impose constraints only in the pixel space, as we found that this setup, combined with JND modulation, already achieves high visual quality. Introducing constraints in the feature space or using GAN-based losses would negatively impact the overall performance, as discussed in Sec. 4.5.

The decoder loss is formulated as:

$$\mathcal{L}_{dec} = \mathcal{L}_{MSE}(W_{pd}, W_{gt}) + \alpha \mathcal{L}_{MSE}(M_{pd}, M), \quad (5)$$

where  $\alpha$  is a factor controlling the weight of the mask loss. The overall objective function is:

$$\mathcal{L}_{total} = \beta_{enc} \cdot \mathcal{L}_{enc} + \beta_{dec} \cdot \mathcal{L}_{dec}, \quad (6)$$

where  $\beta_{enc}$  and  $\beta_{dec}$  are the weights for the encoder and decoder losses, respectively.

Compared to conventional watermarking methods, our approach introduces only a mask loss at the decoder stage. As a result, the method retains a simple yet effective objective, making it easy to extend.

### 3.8 Usage Scenarios

The following section outlines the usage scenarios for the two variants, MaskMark-D and MaskMark-ED, highlighting their distinct watermark embedding strategies tailored to different protection needs. While MaskMark-D is designed for comprehensive image protection, MaskMark-ED focuses on safeguarding specific regions of interest.

**MaskMark-D.** MaskMark-D operates without a mask in the encoder, supporting global watermark embedding and local watermark extraction. The mask is introduced only during decoder training, enabling selective focus on watermarked regions for accurate extraction. This makes MaskMark-D ideal for full-image protection. Even in cases of heavy tampering, where only part of the watermark remains, MaskMark-D can still extract the watermark and identify tampered areas. Its robustness under such conditions makes it a reliable solution for comprehensive image protection.

**MaskMark-ED.** In contrast, MaskMark-ED uses a mask in the encoder, allowing for localized watermark embedding and extraction. This approach is best suited for protecting specific, valuable regions of an image, rather than the entire image. The focus is not on tamper localization across the whole image but on ensuring that key content can be traced if extracted and misused. This targeted protection makes MaskMark-ED ideal for scenarios where only particular regions need safeguarding against unauthorized use.

## 4 Experiments

### 4.1 Implementation Details

For all experiments, we train MaskMark on 83k images from the MS-COCO (Lin et al., 2014) 2014 training set. All images are resized and center-cropped to  $256 \times 256$ . Training is conducted for 100k steps with a batch size of 16 on a single NVIDIA A6000 GPU. We use the AdamW optimizer with a learning rate of  $1 \times 10^{-4}$ , and apply a cosine learning rate scheduler with 2k warm-up steps. We adopt an easy-to-hard training strategy inspired by TrustMark (Bui et al., 2023). During the first 0.5k

steps, the mask is set to full (i.e., all ones) and no distortion is applied. From step 0.5k to 1k, we introduce all types of masks. After 1k steps, distortions are added. The encoder loss weight  $\beta_{enc}$  is fixed at 1, while the decoder loss weight  $\beta_{dec}$  is initially set to 20 and linearly decayed to 0.2 over the first 5k steps. The mask loss weight  $\alpha$  is set to 0.5. The JND module in the encoder is introduced and tuned starting from step 5k, with the scaling factor  $\mu$  set to 1. The details of the distortion pool used during training are provided in Appendix A.1.

For evaluation, we fix the image resolution to  $512 \times 512$ . If a baseline method does not support this resolution, we adopt the resolution scaling strategy from TrustMark (Bui et al., 2023) to interpolate the watermark strength, which preserves watermarking performance. To ensure comparable visual fidelity across variants, we set the JND scaling factor  $\mu$  for MaskMark-D and MaskMark-ED to 1.3 and 1.75, respectively. For robustness evaluation, we separately assess valuemetric and geometric distortions. For valuemetric robustness, we randomly sample from a set of ten common distortions, including JPEG Compression, Gaussian Filter, Gaussian Noise, Median Filter, Salt&Pepper Noise, Resize, Brightness, Contrast, Hue, and Saturation. For geometric robustness, we randomly sample from three typical transformations: Rotation, Perspective, and Horizontal Flip. These distortions collectively cover the vast majority of real-world transformations that watermarked images are likely to encounter in practical scenarios. Detailed parameter settings for each distortion are provided in Appendix A.2.

## 4.2 Global and Local Watermarking Comparison

**Settings.** We compare MaskMark against seven recent open-source watermarking methods with state-of-the-art performance. Among them, StegaStamp (Tancik et al., 2020), SepMark (Wu et al., 2023), TrustMark (Bui et al., 2023), EditGuard (Zhang et al., 2024b), Robust-Wide (Hu et al., 2024b), and VINE (Lu et al., 2024) are designed for global watermarking. WAM (Sander et al., 2025), on the other hand, is a dedicated method for local watermarking. For EditGuard, we evaluate two publicly available variants: the clean version (EditGuard-C), trained without noise augmentation, and the degraded version (EditGuard-D), trained with noise. For VINE, we use the more robust variant, VINE-R.

For global watermarking evaluation, we randomly select 1k images from the MS-COCO 2014 validation set. We use PSNR and SSIM to assess the visual quality of the watermarked images, and Bit Accuracy to evaluate the watermark extraction performance. For local watermarking evaluation, we split the 41k images in the MS-COCO 2014 validation set into 12 subsets based on the ratio of the masked area to the entire image: 1–5%, 5–10%, 10–20%, ..., 80–90%, 90–95%, and 95–99%. From each subset, we randomly select 400 images and then invert the masked regions to simulate both inpainting and outpainting scenarios. That is, if the original masked area is  $a-b\%$ , the inverted masked area will cover  $(100-b)-(100-a)\%$  of the image. This results in  $400 \times 2 = 800$  images per subset, yielding a total of  $800 \times 12 = 9600$  image-mask pairs for evaluation. By default, MaskMark is configured to embed 32 bits for fair comparison with WAM. This capacity is generally sufficient for local watermark embedding and extraction. However, unlike WAM, MaskMark is not restricted to 32-bit capacity. We provide additional results for varying bit lengths in Sec. 4.5.

For the baseline methods and our MaskMark-D, we embed watermark bits across the entire image and then replace the unmasked regions with the corresponding original pixels to obtain the final local watermarked image. In contrast, our MaskMark-ED leverages the mask to embed watermark bits only within the masked region, and similarly replaces the unmasked areas with original pixels, ensuring that the resulting image contains localized watermarking restricted to the target area.

**Global Watermarking Results.** The global watermarking results for all methods are summarized in Table 1. First, both MaskMark-D and MaskMark-ED achieve high visual fidelity, with PSNR scores above 39.5 and SSIM scores exceeding 0.98. These results outperform WAM and are only marginally lower than TrustMark and Robust-Wide. More importantly, under this high-fidelity setting, both variants of MaskMark still maintain near 100% bit accuracy, even under various valuemetric and geometric distortions. This demonstrates significantly better robustness compared to both global and local watermarking baselines. Notably, geometric distortions pose a considerable challenge for existing global watermarking methods, often leading to failure. In contrast, our MaskMark framework remains robust and reliable in such scenarios.

Table 1: Comparison with other baseline watermarking methods in terms of global watermarking. The **best** and the second best results are highlighted in bold and underlined, respectively.

Method	Bit Length	PSNR $\uparrow$	SSIM $\uparrow$	No Distortion $\uparrow$	Distortions	
					Valuemetric $\uparrow$	Geometric $\uparrow$
<i>Global Watermarking Methods</i>						
StegaStamp	100	28.87	0.9019	0.9990	0.9976	0.6646
SepMark	30	35.73	0.9876	0.9957	0.9643	0.5086
TrustMark	100	<u>41.19</u>	<u>0.9922</u>	0.9996	0.9955	0.7868
EditGuard-C	64	<u>37.27</u>	0.9332	0.9991	0.5482	0.4925
EditGuard-D	64	32.30	0.8199	<u>0.9999</u>	0.5444	0.4975
Robust-wide	64	<b>41.58</b>	<b>0.9923</b>	<b>1.0000</b>	0.9944	0.4951
VINE	100	36.04	0.9874	0.9997	<u>0.9986</u>	0.5012
<i>Local Watermarking Methods</i>						
WAM	32	39.32	0.9791	<b>1.0000</b>	0.9986	0.8979
MaskMark-D	32	39.55	0.9814	<b>1.0000</b>	<b>1.0000</b>	0.9998
MaskMark-ED	32	39.52	0.9828	<b>1.0000</b>	<b>1.0000</b>	<b>1.0000</b>

**Local Watermarking Results.** The local watermarking results for all methods are presented in Figure 2. First, we observe that the extraction accuracy of global watermarking methods drops significantly as the watermarked region becomes smaller. This highlights their limitation in handling local watermarking tasks, especially when only a small portion of the image contains the watermark. In contrast, both WAM and our proposed MaskMark maintain high extraction accuracy even when the watermarked area is limited. Among them, MaskMark consistently outperforms WAM, with a more pronounced advantage under distortion scenarios, demonstrating its superior robustness and reliability in practical settings. Finally, comparing our two variants, MaskMark-ED performs better than MaskMark-D when the watermark region is small. As the watermarked area increases, the performance gap between the two variants narrows.

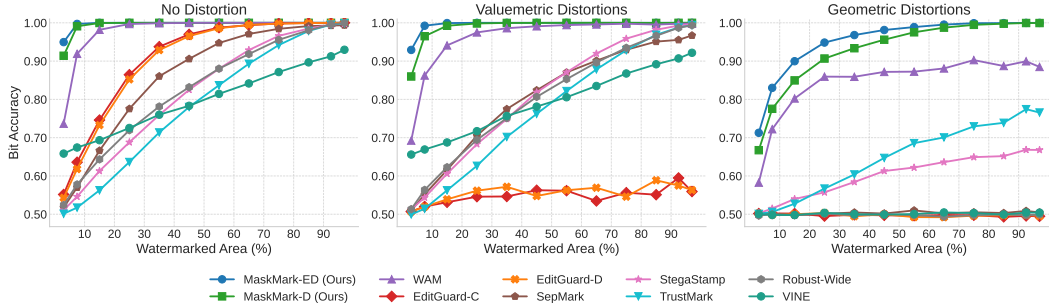


Figure 2: Watermark extraction performance of different methods under different ratios of watermarked area. The intervals of ratios are: 1-5%, 5-10%, ..., 95-99%, 99-100%. We select the average value for each interval's ratios to stand for the interval (e.g., 3% for 1-5%).

The visualized watermark patterns embedded by MaskMark-D and MaskMark-ED are shown in Figure 3, with additional results provided in Appendix B.1.

### 4.3 Watermark Localization Comparison

**Settings.** We compare MaskMark with EditGuard (Zhang et al., 2024b) and WAM (Sander et al., 2025), two methods with watermark localization capabilities, selected from our earlier baseline comparisons in Sec. 4.2. Localization performance is evaluated using the local watermarking dataset described in Sec. 4.2, with Intersection-over-Union (IoU) metrics computed between the predicted and ground-truth regions for both the watermarked and unwatermarked areas.

**Results.** The localization results of different methods are presented in Figure 4. First, our method MaskMark consistently achieves the best localization performance across nearly all watermark ratios and distortion conditions, with WAM showing a noticeable performance gap and EditGuard

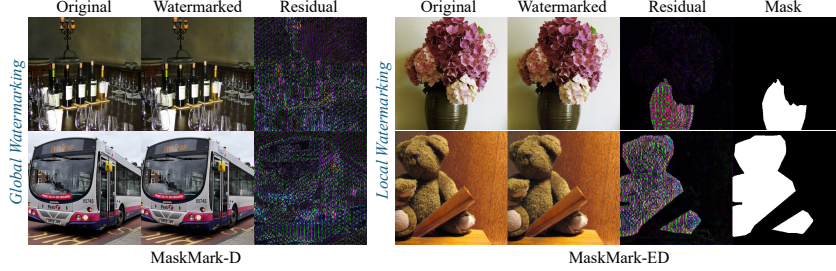


Figure 3: Visualization results of global watermark embedding using MaskMark-D and local watermark embedding using MaskMark-ED.

performing significantly worse. Second, MaskMark-ED achieves better localization accuracy in watermarked regions than MaskMark-D when the watermarked area is small, while MaskMark-D demonstrates superior performance in localizing unwatermarked regions when the watermarked area is large. This trend becomes more pronounced under distortion conditions. An interesting observation is that EditGuard-C exhibits an abnormal increase in localization accuracy for unwatermarked regions as the watermarked area becomes larger, a behavior not seen in EditGuard-D. We hypothesize that this may be due to overfitting: since EditGuard-C is trained solely on clean images without distortions, it may become overly sensitive to specific patterns present in undistorted data. The visualized localization results of different methods are shown in Figure 5, with additional results provided in Appendix B.2.

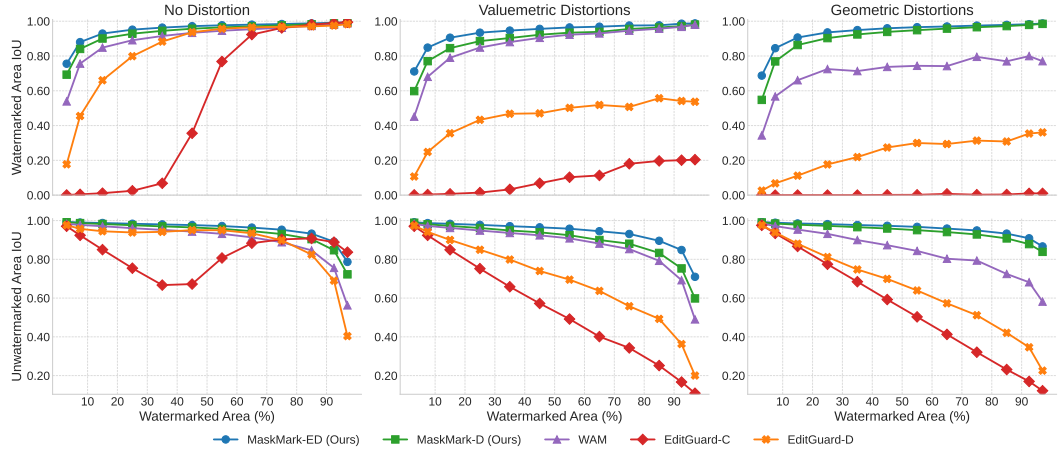


Figure 4: Localization performance of different methods under different ratios of watermarked area.

#### 4.4 Multiple Watermarks Embedding Comparison

**Settings.** We compare the performance of our MaskMark-ED with WAM (Sander et al., 2025) in a multi-watermark embedding setting. Following WAM’s setup, we embed different watermarks into 1–5 non-overlapping square-masked regions to evaluate performance as the number of embedded watermarks increases. These masks are placed at the center, top-left, top-right, bottom-left, and bottom-right positions, forming a checkerboard-like pattern when all five regions are used (see Appendix B.3). Unlike WAM, which assigns 10% of the image area to each mask, we limit each mask to just 5%, making the task significantly more challenging. For each watermark count from 1 to 5, we randomly sample 400 images from the MS-COCO 2014 validation set for evaluation. Performance is assessed using the average watermark extraction accuracy across multiple embedded watermarks and the mean IoU of the predicted watermark regions. For our MaskMark-ED model, we apply OpenCV’s `cv2.connectedComponents` function to segment the extracted mask into disjoint regions, allowing independent watermark extraction from each region.

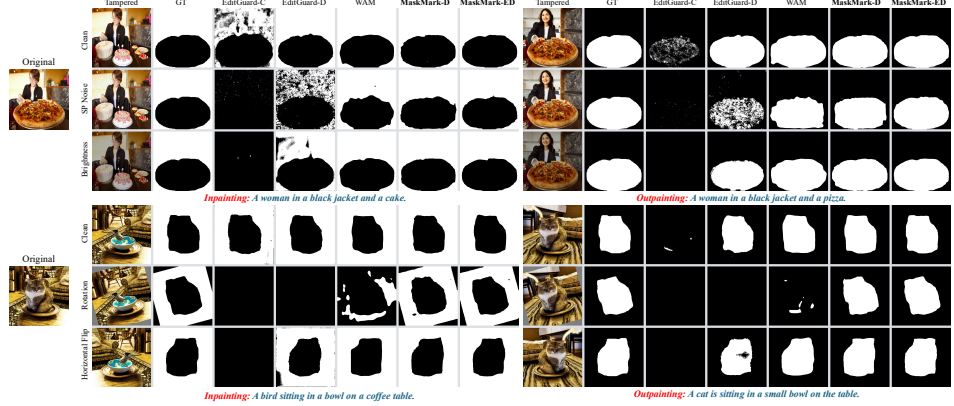


Figure 5: Visualization results of watermark localization using different methods. The inpainting and outpainting results are obtained by applying *stable-diffusion-2-inpainting* (Rombach et al., 2022) to the masked regions for content reconstruction.

**Results.** Figure 6 presents the comparison results. First, our MaskMark-ED consistently outperforms WAM in both watermark extraction and localization, across all tested numbers of embedded watermarks and under various distortion conditions. Second, despite being trained solely with single-watermark supervision, MaskMark-ED generalizes well to multi-watermark settings, demonstrating strong scalability. Under geometric distortions, we observe a degradation in extraction accuracy as the number of embedded watermarks increases. This is primarily due to the spatial transformations disproportionately shrinking the watermark regions located in the image corners, thereby reducing the effective area available for extraction (see Appendix B.3).

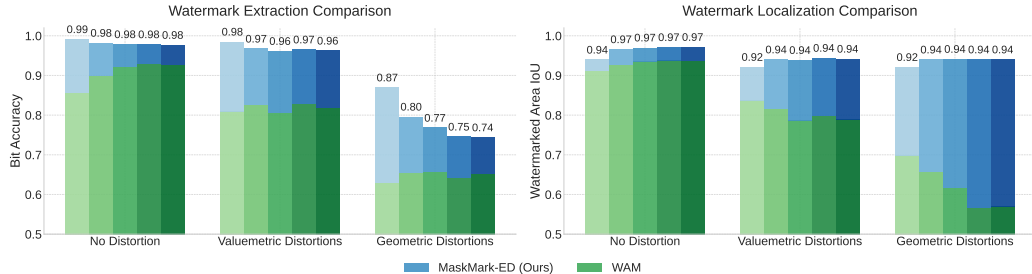


Figure 6: Performance comparison of watermark extraction and localization when embedding multiple watermarks. The bar colors transition from light to dark from left to right, representing the embedding of 1 to 5 different bit strings in a single image.

#### 4.5 More Analysis

**Scalability to Different Watermark Bit Lengths.** Unlike WAM (Sander et al., 2025), our MaskMark can be readily scaled to support longer watermark bit lengths. As shown in Figure 7, MaskMark maintains high extraction accuracy across various bit lengths. Even at 64 bits, the accuracy experiences only a slight drop and still outperforms WAM at 32 bits. While the accuracy decline becomes more noticeable at 128 bits, MaskMark consistently surpasses WAM under both no distortion and valuemetric distortion conditions. The only exception arises under geometric distortion, where a performance gap emerges when the watermark region covers between 5% and 75%. These results underscore the scalability and optimization-friendly design of our method, emphasizing its practical advantages.

**Effects of Different Visual Quality Enhancement Methods.** Our experiments demonstrate that using only an MSE loss in pixel space to constrain the difference between the watermarked and original images (referred to as the Base version) already yields high PSNR and SSIM scores. However,

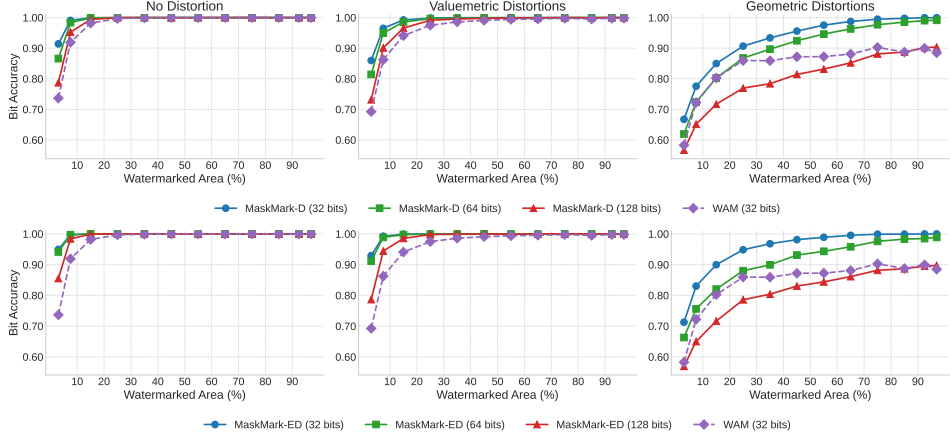


Figure 7: Watermark extraction performance of MaskMark-D and MaskMark-ED with different bits length. We also put the results of WAM for comparison.

despite the favorable metrics, the resulting images often contain visible artifacts that may compromise perceived visual quality. To address this issue, we investigate several enhancement strategies: (1) incorporating a GAN (Isola et al., 2017) loss, (2) adding a perceptual constraint via LPIPS (Zhang et al., 2018) loss in the feature space, and (3) modulating the watermark signal using a Just Noticeable Difference (JND) (Wu et al., 2017) module. We conduct experiments on the MaskMark-D variant, but the findings similarly hold for MaskMark-ED.

As illustrated in Figure 8, when the weights of the GAN and LPIPS losses are small, they are insufficient to suppress artifacts effectively. Increasing these weights helps reduce artifacts but negatively impacts the performance of local watermark extraction and localization (see Figure 18 in Appendix B.4 for detailed results). In contrast, applying JND-based modulation proves more effective: it significantly reduces visible artifacts while maintaining performance comparable to the Base version. These findings suggest that, unlike global perceptual losses such as GAN or LPIPS, JND offers a more adaptive and content-aware modulation strategy. It effectively suppresses visual artifacts while preserving the watermark’s integrity, making it a practical choice for visual quality enhancement.

**Enhancing Robustness Against Adaptive Attacks via Fast Fine-tuning.** Although MaskMark is trained with a broad set of common valuemetric and geometric distortions, it is impractical to account for all possible types of distortions during training. Fortunately, the flexibility of our framework allows users to easily perform task-specific enhancement and fine-tuning based on their particular needs. As a demonstration, we target a recently popular class of VAE-based adaptive attacks (Kingma & Welling, 2014), which use variational autoencoders to reconstruct images and potentially erase embedded watermark signals. Specifically, we expand the distortion pool during fine-tuning by incorporating VAE modules from Stable Diffusion v1-4 (Rombach et al., 2022), Bmshj18 (Ballé et al., 2018), and Cheng20 (Cheng et al., 2020). These VAE-based distortions are applied with a probability of 50%, while the original distortion types are retained with the remaining 50%. The hyperparameters are configured as follows:  $\beta_{\text{dec}} = 0.3$ , learning rate =  $1 \times 10^{-4}$ , and the quality levels for *Bmshj18* and *Cheng20* are set to 5.

We find that fine-tuning for 20k steps on a single A6000 GPU, approximately 5 hours, is sufficient to achieve strong performance. As shown in Figure 9, the fine-tuned MaskMark exhibits significantly enhanced robustness against VAE-based attacks, clearly outperforming existing baselines. However, we also observe a slight drop in robustness against other types of distortions. Despite this trade-off, MaskMark still maintains superior performance compared to existing methods overall. This highlights the adaptability of our approach, enabling users to make informed trade-offs based on their specific application requirements.

**Importance of Localization Before Extracting Local Watermarks.** We evaluate watermark extraction performance using three types of masks during decoding: a full mask, a predicted mask,

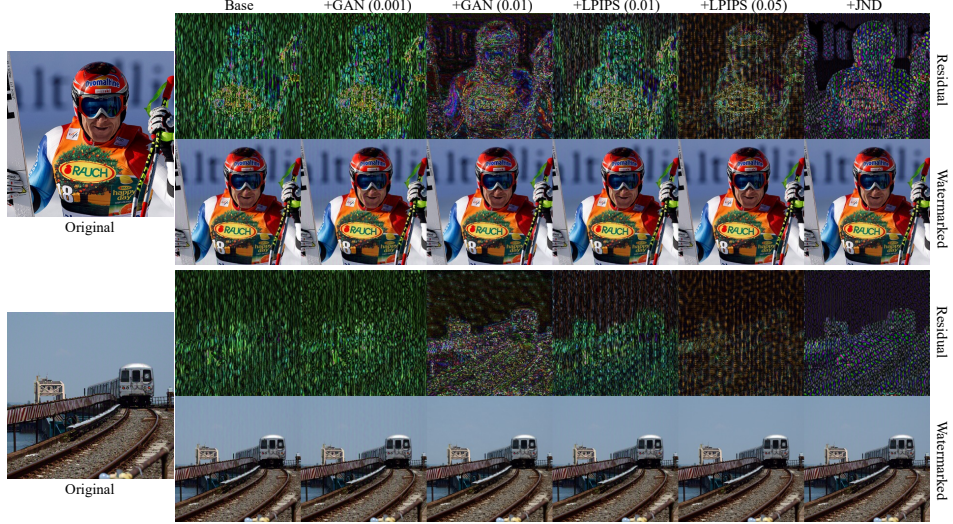


Figure 8: Visualization results of watermark using different visual quality enhancement methods. The residual image is acquired by  $10 \times |I_{wm} - I_{orig}|$  for observation. Zoom in to see more details. The numbers in parentheses indicate the corresponding loss weights. For example, GAN (0.001) means the GAN loss is assigned a weight of 0.001 in the total loss function, i.e.,  $\mathcal{L}_{\text{total}} = \beta_{\text{enc}}\mathcal{L}_{\text{enc}} + \beta_{\text{dec}}\mathcal{L}_{\text{dec}} + 0.001\mathcal{L}_{\text{GAN}}$ , and LPIPS (0.01) indicates that the LPIPS loss is weighted by 0.01, i.e.,  $\mathcal{L}_{\text{enc}} = \mathcal{L}_{\text{MSE}}(I_{wm}, I_{orig}) + 0.01\mathcal{L}_{\text{LPIPS}}$ . To ensure a fair comparison, we adjust either the strength of the added watermark residual or the JND modulation coefficient to maintain comparable PSNR and SSIM across different settings.

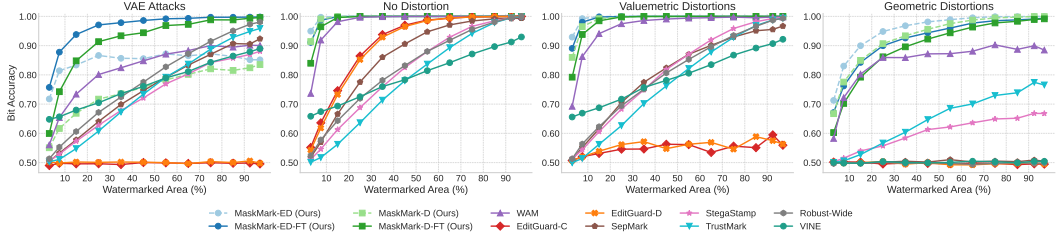


Figure 9: The effect of VAE fine-tuning on the robustness of our MaskMark. Fine-tuning the VAE enhances robustness against VAE attacks, with minimal impact on the original robustness performance.

and a ground-truth mask. With the full mask, the entire image is passed to the decoder for extraction. The predicted mask retains only the regions identified as containing the watermark, setting the pixel values of all other regions to zero. The ground-truth mask isolates the actual watermark-containing regions based on annotation.

As shown in Figure 10, when the watermark is embedded in small, localized regions, using the full mask leads to significantly lower extraction accuracy. In contrast, the predicted mask yields a notable improvement, and the ground-truth mask further boosts performance. These results indicate that removing irrelevant image content helps reduce interference, thereby enhancing local watermark extraction. They also underscore the importance of performing localization prior to extraction in scenarios involving spatially localized watermarks.

**Computation Overhead Evaluation.** We compare MaskMark with EditGuard and WAM, both of which support watermark extraction and localization, in terms of training and inference costs. The results are summarized in Table 2. First, in terms of model size, MaskMark has fewer parameters than WAM, with the encoder and decoder having comparable sizes. In contrast, WAM allocates most of its parameters to the decoder, as its decoding task is inherently more complex. Second, regarding

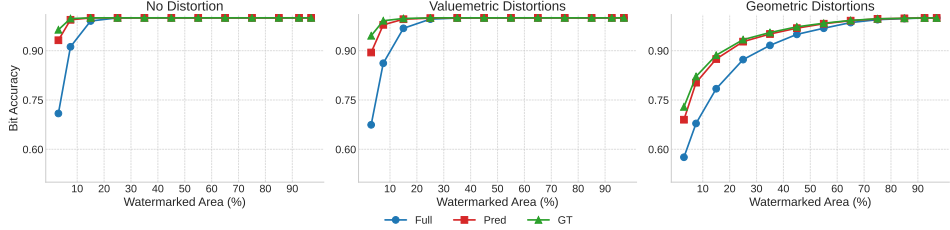


Figure 10: Watermark extraction performance using different masking strategies during decoding.

training overhead, MaskMark is significantly more efficient than WAM. Measured in TFLOPs, the training cost of MaskMark is approximately 1/15 that of WAM. Although EditGuard does not report explicit training overhead, it is noteworthy that even without incorporating strong distortions for robustness during training, its total data consumption (steps  $\times$  batch) already amounts to 60% of ours. Finally, for inference overhead, despite having fewer parameters, EditGuard embeds both localization and copyright watermarks into the image, which substantially increases both memory usage and inference time. In contrast, MaskMark and WAM incur much lower inference latency and exhibit similar memory consumption.

Table 2: Training and inference costs of different methods. The inference time is evaluated on a single A6000 with a batch size of 1 by averaging the total processing time over 1000 images.

Method	# Params (M)			Train					Inference				
	Enc	Dec	Total	Steps	Batch	GPU	Time	TFLOPs	Memory	Enc Time	Dec Time	Total Time	Memory
EditGuard	3.6	2.6	6.2	25w	4	-	-	-	-	0.074 s	0.080 s	0.154 s	2.15 GB
WAM	1.1	96.0	97.1	368w	16	8 V100	90 h	$1.13 \times 10^{16}$	-	0.015 s	0.017 s	0.032 s	2.33 GB
MaskMark	31.1	32.2	63.3	10w	16	1 A6000	20 h	$7.74 \times 10^{14}$	25.84 GB	0.009 s	0.022 s	0.031 s	2.21 GB

## 5 Conclusion

We propose MaskMark, a simple, efficient, and flexible framework for image watermarking that supports both global and local watermark embedding, extraction, and localization. It enables applications such as tamper detection and localized image protection. Built on the classical Encoder-Distortion-Decoder paradigm, MaskMark introduces a masking mechanism and a localization module to facilitate accurate and robust watermark extraction, especially in local regions. Extensive experiments demonstrate that MaskMark achieves state-of-the-art performance across all major tasks while maintaining high visual quality and significantly reducing computational cost. We hope MaskMark can serve as a strong foundation and inspire future research in image watermarking.

## References

Johannes Ballé, David Minnen, Saurabh Singh, Sung Jin Hwang, and Nick Johnston. Variational image compression with a scale hyperprior. In *International Conference on Learning Representations*, 2018.

Tu Bui, Shruti Agarwal, and John Collomosse. Trustmark: Universal watermarking for arbitrary resolution images. *arXiv preprint arXiv:2311.18297*, 2023.

Zhengxue Cheng, Heming Sun, Masaru Takeuchi, and Jiro Katto. Learned image compression with discretized gaussian mixture likelihoods and attention modules. In *Proceedings of the IEEE/CVF conference on computer vision and pattern recognition*, pp. 7939–7948, 2020.

Han Fang and et al. Pimog: An effective screen-shooting noise-layer simulation for deep-learning-based watermarking network. In *ACM MM*, pp. 2267–2275, 2022.

Runyi Hu, Jie Zhang, Yiming Li, Jiwei Li, Qing Guo, Han Qiu, and Tianwei Zhang. Supermark: Robust and training-free image watermarking via diffusion-based super-resolution. *arXiv preprint arXiv:2412.10049*, 2024a.

Runyi Hu, Jie Zhang, Ting Xu, Jiwei Li, and Tianwei Zhang. Robust-wide: Robust watermarking against instruction-driven image editing. In *European Conference on Computer Vision*, pp. 20–37. Springer, 2024b.

Runyi Hu, Jie Zhang, Yiming Li, Jiwei Li, Qing Guo, Han Qiu, and Tianwei Zhang. Videoshield: Regulating diffusion-based video generation models via watermarking. In *International Conference on Learning Representations (ICLR)*, 2025.

Phillip Isola, Jun-Yan Zhu, Tinghui Zhou, and Alexei A Efros. Image-to-image translation with conditional adversarial networks. In *Proceedings of the IEEE conference on computer vision and pattern recognition*, pp. 1125–1134, 2017.

Zhaoyang Jia, Han Fang, and Weiming Zhang. Mbrs: Enhancing robustness of dnn-based watermarking by mini-batch of real and simulated jpeg compression. In *Proceedings of the 29th ACM international conference on multimedia*, pp. 41–49, 2021.

Diederik P Kingma and Max Welling. Auto-encoding variational bayes. In *Proceedings of the 2nd International Conference on Learning Representations (ICLR)*, 2014.

Alexander Kirillov, Eric Mintun, Nikhila Ravi, Hanzi Mao, Chloe Rolland, Laura Gustafson, Tete Xiao, Spencer Whitehead, Alexander C Berg, Wan-Yen Lo, et al. Segment anything. In *Proceedings of the IEEE/CVF international conference on computer vision*, pp. 4015–4026, 2023.

Tsung-Yi Lin, Michael Maire, Serge Belongie, James Hays, Pietro Perona, Deva Ramanan, Piotr Dollár, and C Lawrence Zitnick. Microsoft coco: Common objects in context. In *Computer Vision–ECCV 2014: 13th European Conference, Zurich, Switzerland, September 6–12, 2014, Proceedings, Part V 13*, pp. 740–755. Springer, 2014.

Shilin Lu, Zihan Zhou, Jiayou Lu, Yuanzhi Zhu, and Adams Wai-Kin Kong. Robust watermarking using generative priors against image editing: From benchmarking to advances. *arXiv preprint arXiv:2410.18775*, 2024.

Vidyasagar M Potdar, Song Han, and Elizabeth Chang. A survey of digital image watermarking techniques. In *INDIN’05. 2005 3rd IEEE International Conference on Industrial Informatics*, 2005., pp. 709–716. IEEE, 2005.

Xuebin Qin, Zichen Zhang, Chenyang Huang, Masood Dehghan, Osmar R Zaiane, and Martin Jagersand. U2-net: Going deeper with nested u-structure for salient object detection. *Pattern recognition*, 106:107404, 2020.

Robin Rombach, Andreas Blattmann, Dominik Lorenz, Patrick Esser, and Björn Ommer. High-resolution image synthesis with latent diffusion models. In *Proceedings of the IEEE/CVF conference on computer vision and pattern recognition*, pp. 10684–10695, 2022.

Olaf Ronneberger, Philipp Fischer, and Thomas Brox. U-net: Convolutional networks for biomedical image segmentation. In *Medical image computing and computer-assisted intervention–MICCAI 2015: 18th international conference, Munich, Germany, October 5–9, 2015, proceedings, part III 18*, pp. 234–241. Springer, 2015.

Chitwan Saharia, William Chan, Saurabh Saxena, Lala Li, Jay Whang, Emily L Denton, Kamyar Ghasemipour, Raphael Gontijo Lopes, Burcu Karagol Ayan, Tim Salimans, et al. Photorealistic text-to-image diffusion models with deep language understanding. *Advances in neural information processing systems*, 35:36479–36494, 2022.

Tom Sander, Pierre Fernandez, Alain Durmus, Teddy Furon, and Matthijs Douze. Watermark anything with localized messages. In *International Conference on Learning Representations (ICLR)*, 2025.

Roman Suvorov, Elizaveta Logacheva, Anton Mashikhin, Anastasia Remizova, Arsenii Ashukha, Aleksei Silvestrov, Naejin Kong, Harshith Goka, Kiwoong Park, and Victor Lempitsky. Resolution-robust large mask inpainting with fourier convolutions. In *Proceedings of the IEEE/CVF winter conference on applications of computer vision*, pp. 2149–2159, 2022.

Matthew Tancik, Ben Mildenhall, and Ren Ng. Stegastamp: Invisible hyperlinks in physical photographs. In *Proceedings of the IEEE/CVF conference on computer vision and pattern recognition*, pp. 2117–2126, 2020.

Jinjian Wu, Leida Li, Weisheng Dong, Guangming Shi, Weisi Lin, and C-C Jay Kuo. Enhanced just noticeable difference model for images with pattern complexity. *IEEE Transactions on Image Processing*, 26(6): 2682–2693, 2017.

Xiaoshuai Wu, Xin Liao, and Bo Ou. Sepmark: Deep separable watermarking for unified source tracing and deepfake detection. In *Proceedings of the 31st ACM International Conference on Multimedia*, pp. 1190–1201, 2023.

Tao Yu, Runseng Feng, Ruoyu Feng, Jimming Liu, Xin Jin, Wenjun Zeng, and Zhibo Chen. Inpaint anything: Segment anything meets image inpainting. *arXiv preprint arXiv:2304.06790*, 2023.

Lijun Zhang, Xiao Liu, Antoni Viros Martin, Cindy Xiong Bearfield, Yuriy Brun, and Hui Guan. Attack-resilient image watermarking using stable diffusion, 2024a.

Lvmin Zhang, Anyi Rao, and Maneesh Agrawala. Adding conditional control to text-to-image diffusion models. In *Proceedings of the IEEE/CVF international conference on computer vision*, pp. 3836–3847, 2023.

Richard Zhang, Phillip Isola, Alexei A Efros, Eli Shechtman, and Oliver Wang. The unreasonable effectiveness of deep features as a perceptual metric. In *Proceedings of the IEEE conference on computer vision and pattern recognition*, pp. 586–595, 2018.

Xuanyu Zhang, Runyi Li, Jiwen Yu, Youmin Xu, Weiqi Li, and Jian Zhang. Editguard: Versatile image watermarking for tamper localization and copyright protection. In *Proceedings of the IEEE/CVF Conference on Computer Vision and Pattern Recognition*, pp. 11964–11974, 2024b.

Xuanyu Zhang, Zecheng Tang, Zhipei Xu, Runyi Li, Youmin Xu, Bin Chen, Feng Gao, and Jian Zhang. Omniduard: Hybrid manipulation localization via augmented versatile deep image watermarking. *arXiv preprint arXiv:2412.01615*, 2024c.

Jiren Zhu, Russell Kaplan, Justin Johnson, and Li Fei-Fei. Hidden: Hiding data with deep networks. In *Proceedings of the European conference on computer vision (ECCV)*, pp. 657–672, 2018.

## A More Details

### A.1 Training

**Valuemetric Distortions.** During training, valuemetric robustness is enhanced by randomly sampling from a set of ten common distortions: JPEG Compression, Gaussian Filter, Gaussian Noise, Median Filter, Salt&Pepper Noise, Resize, Brightness, Contrast, Hue, and Saturation. The distortion parameters are set as follows:

- **JPEG Compression:** quality factor = 50.
- **Gaussian Filter:** kernel size = 1, sigma = 5.
- **Gaussian Noise:** mean = 0, standard deviation = 0.1.
- **Median Filter:** kernel size = 5.
- **Salt&Pepper Noise:** noise ratio = 0.1.

**Geometric Distortions.** To improve geometric robustness, we randomly sample from three typical geometric transformations: Rotation, Perspective, and Horizontal Flip. The specific configurations are:

- **Rotation:** angle sampled from  $[-90^\circ, 90^\circ]$ .
- **Perspective:** distortion scale sampled from  $[0.1, 0.5]$ .
- **Horizontal Flip:** no parameters.

### A.2 Evaluation

**Valuemetric Distortions.** We apply ten valuemetric distortions with the following parameter settings to test generalization:

- **JPEG Compression:** quality factor = 60.
- **Gaussian Filter:** kernel size = 1, sigma = 3.
- **Gaussian Noise:** mean = 0, standard deviation = 0.05.
- **Median Filter:** kernel size = 3.
- **Salt&Pepper Noise:** noise ratio = 0.05.
- **Resize:** scaling factor = 0.5.

- **Brightness Adjustment:** range (0.7, 1.3).
- **Contrast Adjustment:** range (0.7, 1.3).
- **Hue Adjustment:** range (−0.1, 0.1).
- **Saturation Adjustment:** range (0.7, 1.3).

**Geometric Distortions.** We apply three geometric distortions with the following parameter settings to test generalization:

- **Rotation:** angle sampled from  $[-30^\circ, 30^\circ]$ .
- **Perspective:** distortion scale sampled from [0.1, 0.3].
- **Horizontal Flip:** no parameters.

## B More Results

### B.1 Visualization Results of Global and Local Watermark Embedding

See Figure 11.

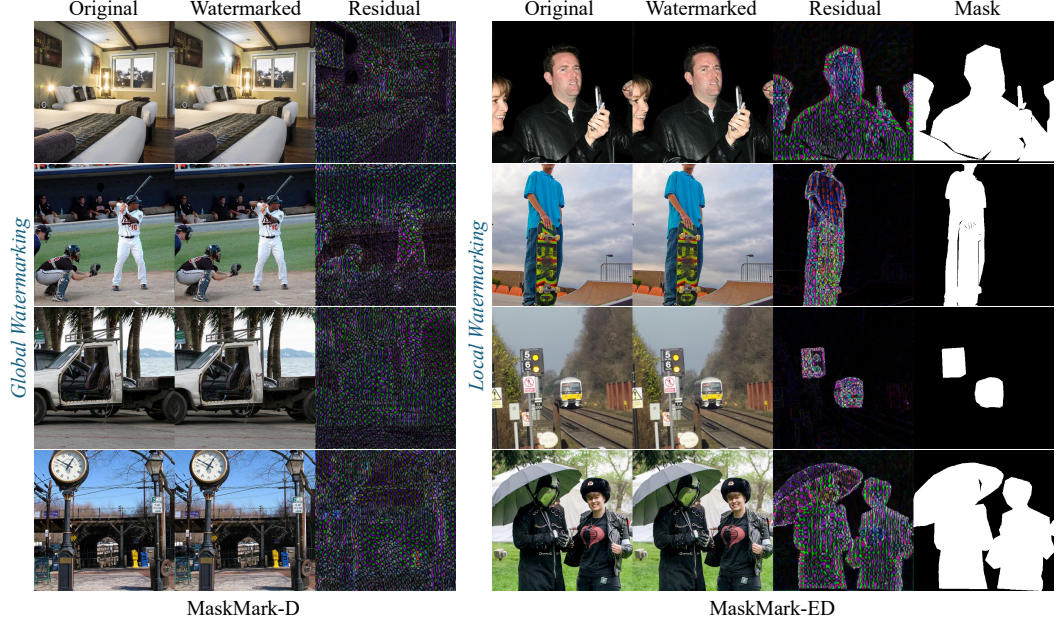


Figure 11: Visualization results of global watermark embedding using MaskMark-D and local watermark embedding using MaskMark-ED.

### B.2 Visualization Results of Localization

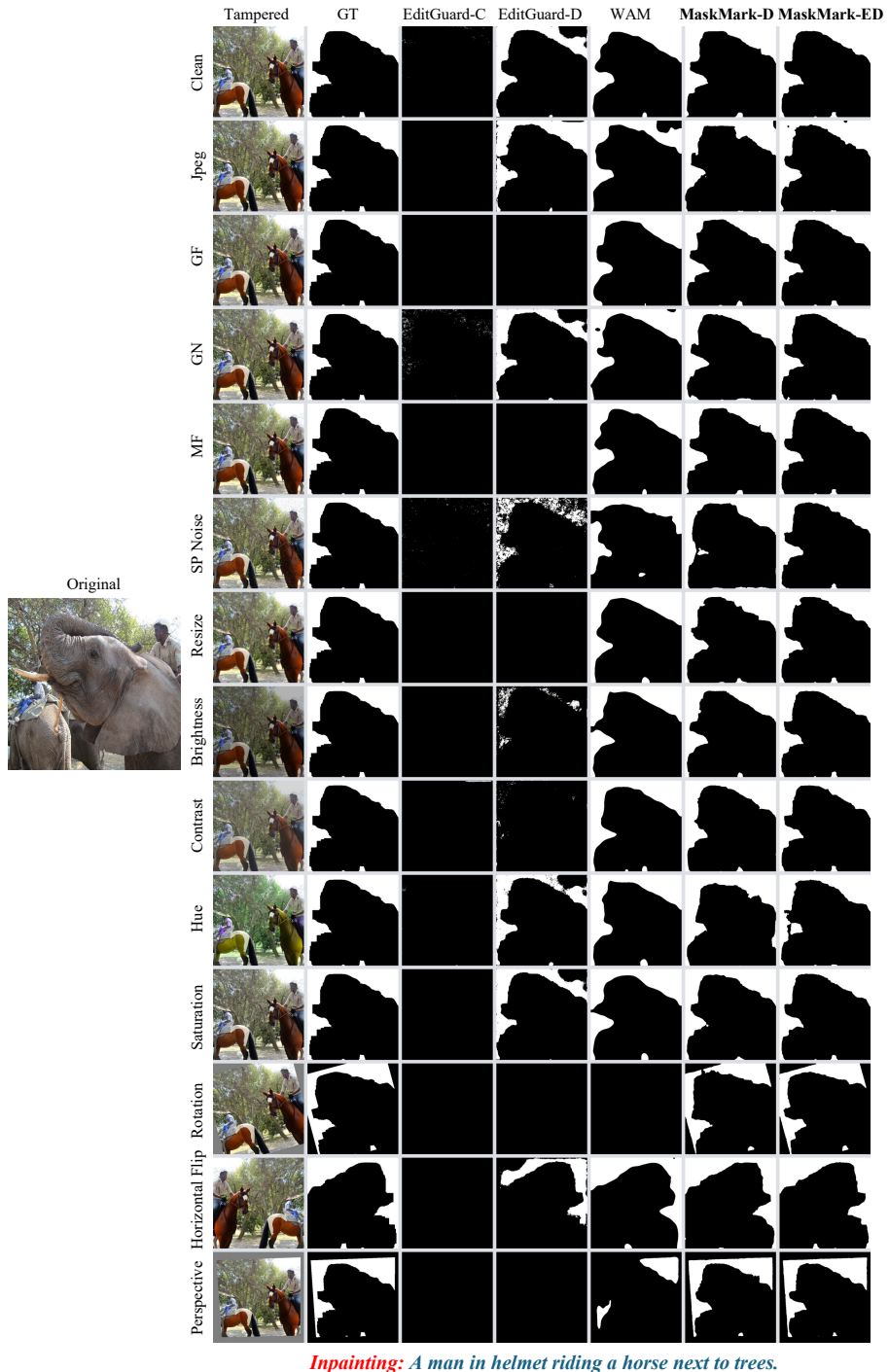
See Figure 12, Figure 13, Figure 14, Figure 15.

### B.3 Visualization Results of Multiple Watermarks Embedding

See Figure 16.

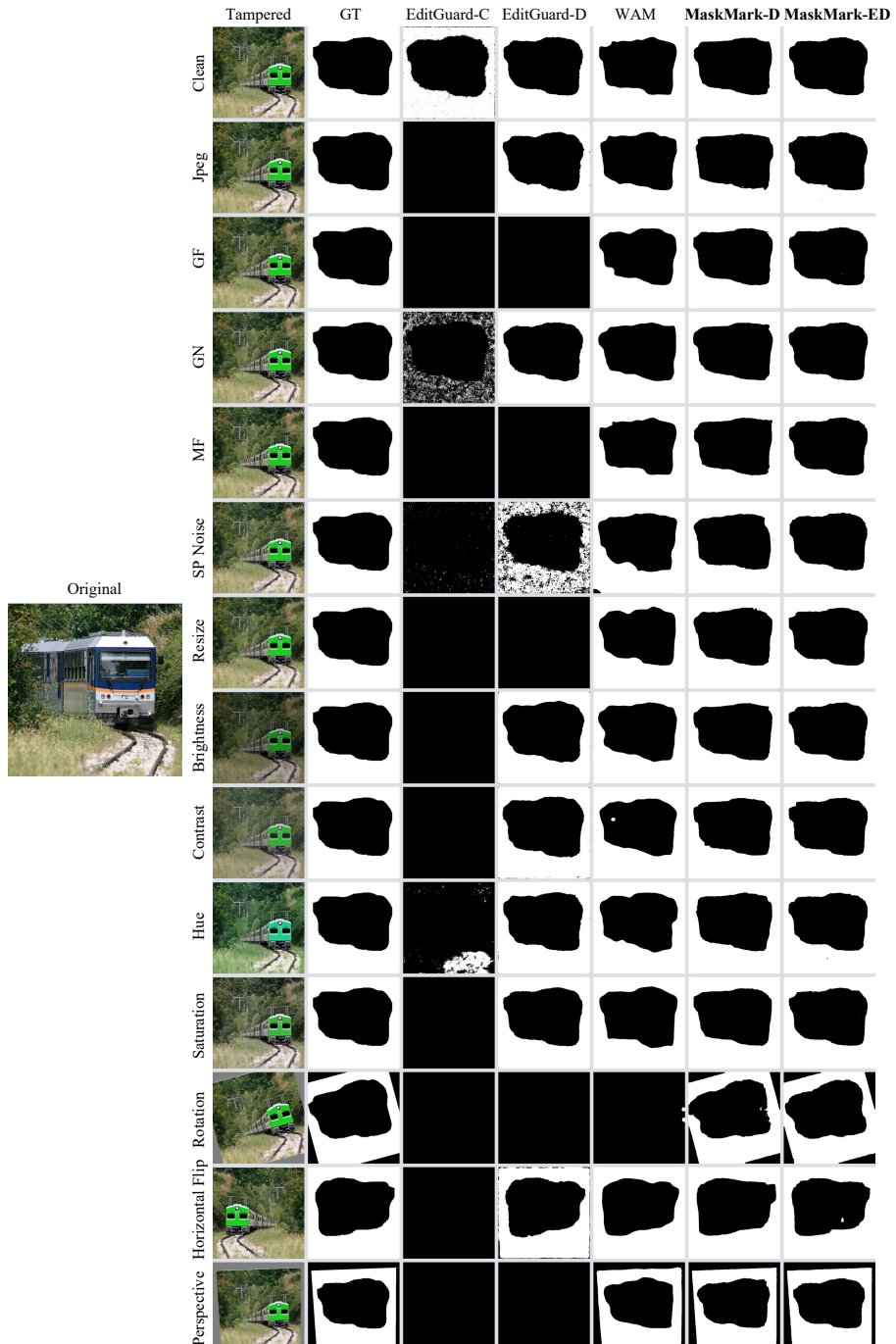
### B.4 Results of MaskMark-D Adopting Different Visual Quality Enhancement Methods

See Figure 17, Figure 18.



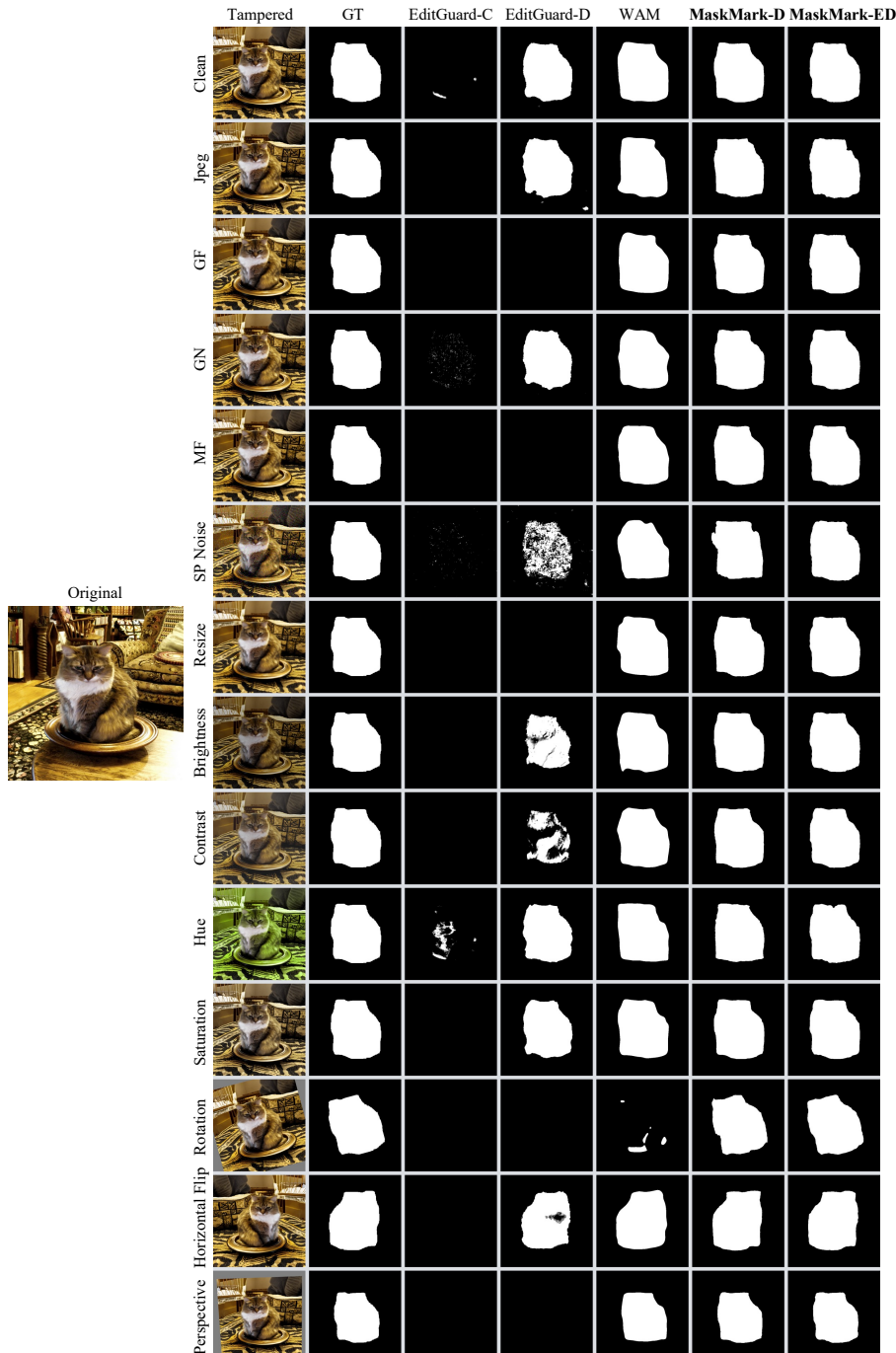
*Inpainting: A man in helmet riding a horse next to trees.*

Figure 12: More visualization results of watermark localization using different methods.



*Inpainting: A green train going up the tracks, lots of trees around.*

Figure 13: More visualization results of watermark localization using different methods.



*Outpainting: A cat is sitting in a small bowl on the table.*

Figure 14: More visualization results of watermark localization using different methods.



*Outpainting: A group of zebra standing on top of a grass covered hillside.*

Figure 15: More visualization results of watermark localization using different methods.

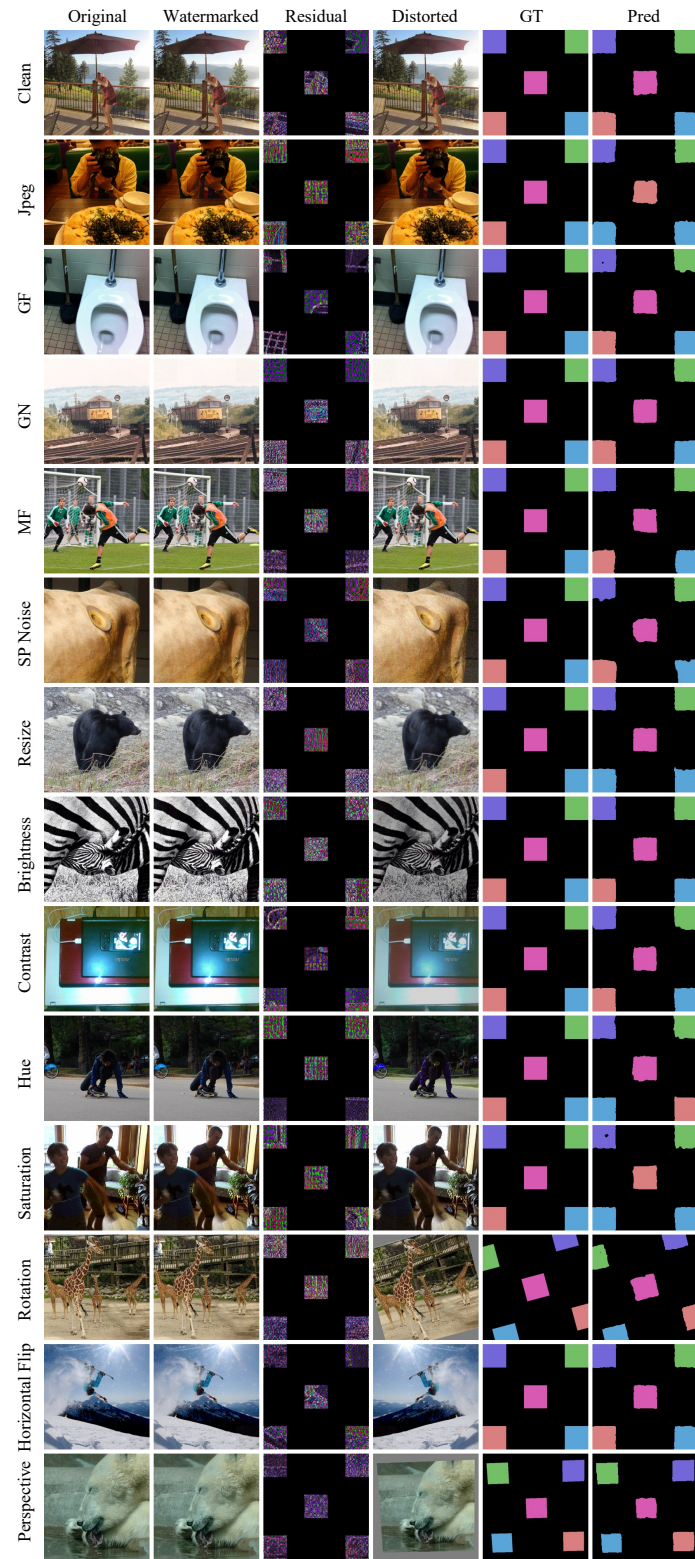


Figure 16: Visualization of multi-watermark embedding and localization results. In the GT column, different colors in the mask indicate different watermark messages.

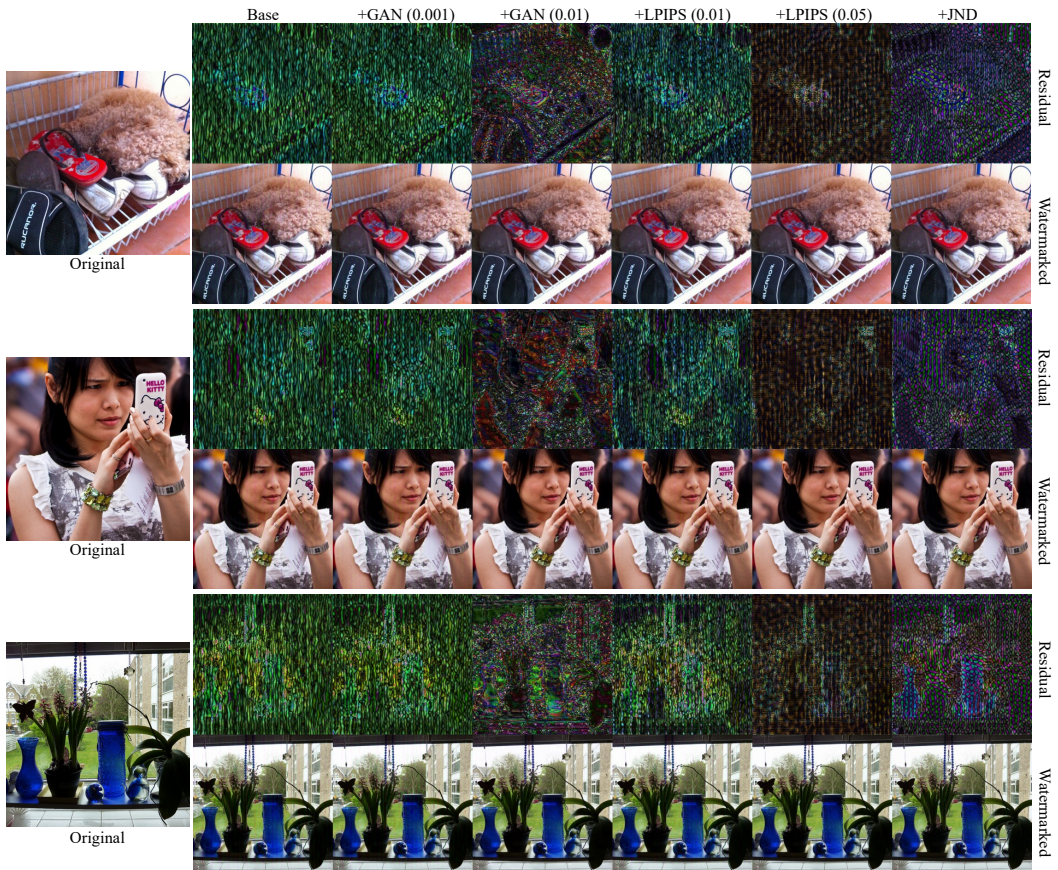


Figure 17: More visualization results of watermark using different visual quality enhancement methods. The residual image is acquired by  $10 \times |I_{wm} - I_{orig}|$  for observation. Zoom in to see more details.

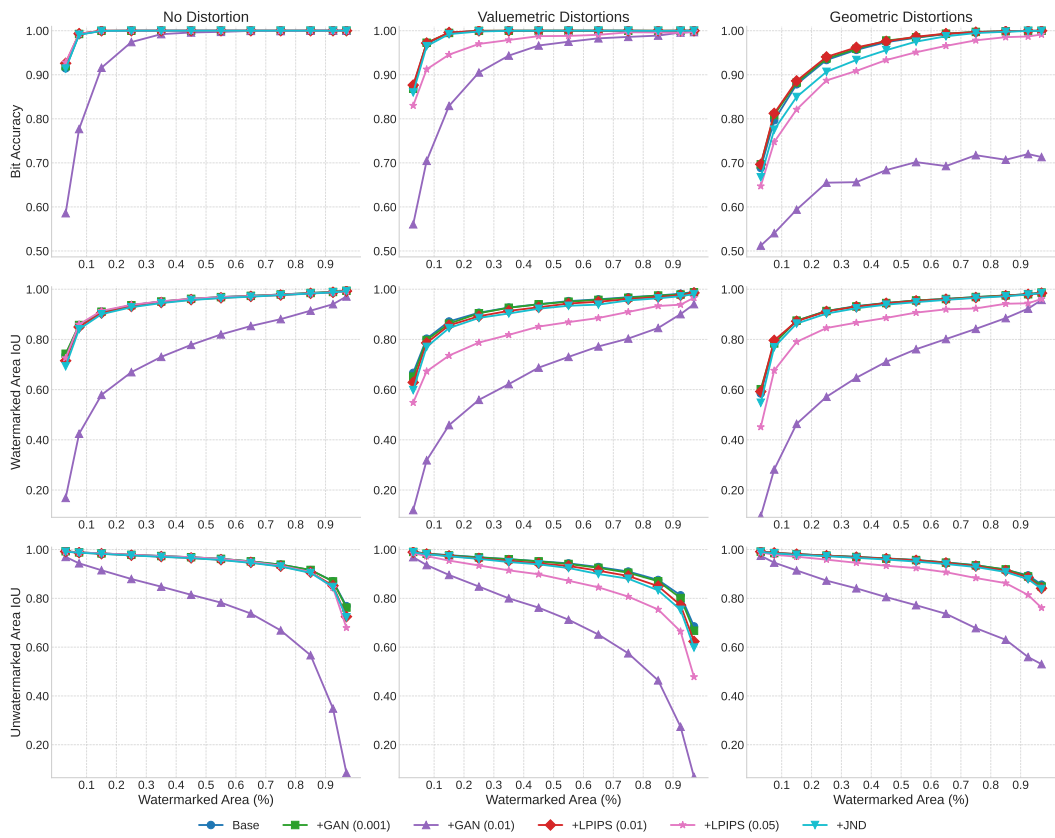


Figure 18: Local watermark extraction and localization performance of MaskMark-D trained with different visual quality enhancement methods.